Available online at www.sciencedirect.com
ScienceDirect
Chinese Journal of Natural Medicines 2020, **18**(1): 57–69
doi: 10.1016/S1875-5364(20)30005-4
Chinese Journal of Natural Medicines

The crucial role of metabolic regulation in differential hepatotoxicity induced by furanoids in *Dioscorea bulbifera*

WU Zi-Tian[1], LI Zhuo-Qing[1], SHI Wei[1], WANG Ling-Li[1], JIANG Yan[2,*], LI Ping[1], LI Hui-Jun[1,*]

[1] *State Key Laboratory of Natural Medicines, China Pharmaceutical University, Nanjing 210009, China;*
[2] *College of Chemical Engineering, Nanjing Forestry University, Nanjing 210037, China*

Available online 20 Jan., 2020

[ABSTRACT] Diterpenoid lactones (DLs), a group of furan-containing compounds found in *Dioscorea bulbifera* L. (DB), have been reported to be associated with hepatotoxicity. Different hepatotoxicities of these DLs have been observed *in vitro*, but reasonable explanations for the differential hepatotoxicity have not been provided. Herein, the present study aimed to confirm the potential factors that contribute to varied hepatotoxicity of four representative DLs (diosbulbins A, B, C, F). *In vitro* toxic effects were evaluated in various cell models and the interactions between DLs and CYP3A4 at the atomic level were simulated by molecular docking. Results showed that DLs exhibited varied cytotoxicities, and that CYP3A4 played a modulatory role in this process. Moreover, structural variation may cause different affinities between DLs and CYP3A4, which was positively correlated with the observation of cytotoxicity. In addition, analysis of the glutathione (GSH) conjugates indicated that reactive intermediates were formed by metabolic oxidation that occurred on the furan moiety of DLs, whereas, GSH consumption analysis reflected the consistency between the reactive metabolites and the hepatotoxicity. Collectively, our findings illustrated that the metabolic regulation played a crucial role in generating the varied hepatotoxicity of DLs.

[KEY WORDS] *Dioscorea bulbifera*; Diterpenoid lactones; Metabolic regulation; Hepatotoxicity; Furan moiety
[CLC Number] R965 **[Document code]** A **[Article ID]** 2095-6975(2020)01-0057-13

Introduction

Furan is a powerful toxin used in the synthesis of pharmaceuticals. With the increasing focus on drug safety issues, the cases of severe adverse effects caused by furan, particularly hepatotoxicity, have been frequently reported [1-2]. The furan ring moiety is considered to be a structure that is flagged with an alert for medicinal chemists and risk assessors [3]. Naturally, there has been concern regarding furan-containing Chinese herbal medicines (CHMs) because the applications of CHMs have been increased for the prevention and treatment of various illnesses. Several studies have confirmed that furan-containing compounds, *viz*. (*R*)-(+)-menthofuran [4-5], toosendanin [6] and dictamnine [7] are responsible for the CHMs-induced liver injuries. However, not all furan-containing molecules are toxic [8]. Some furan-containing compounds in CHMs exhibit strong hepatoprotective activities, anti-inflammatory activities [9] and activation of osteoblasts [10]. Therefore, clarifying the general mechanism of the toxicity and providing reasonable explanations for the varied toxic effects among these furan-containing compounds are necessary.

The tuber of *Dioscorea bulbifera* L. (DB) (Fig. 1A), termed as "huangyaozi" in Chinese, has been widely used in China as a treatment for tumors, cancers and thyroid gland diseases [11-12]. Nevertheless, a series of reports have recently demonstrated that long-term and excessive use of DB could cause severe hepatotoxicity [13-14]. Among the components isolated and characterized from DB, it was determined that the diterpenoid lactones (DLs) containing a furan ring, namely diosbulbins A–P (DIOA–DIOP) and 8-*epi*-diosbulbin E acetate [15-16] may cause potential hepatotoxicity. It is widely accepted that furan is metabolically activated to reactive intermediate *via* a cytochrome P450-dependent process [17-18] and the intermediate reacts with cellular proteins or nucleophiles to exert toxicity [19]. Similarly, as the most abundant DL in DB, DIOB has been confirmed as one of the main hepatotoxic constituents [20]. Current studies have demonstrated that hepatotoxicity elicited by diosbulbin B is

[Received on] 03-Aug.-2019
[Research funding] This work was supported by the National Natural Science Foundation of China (No. 81773993).
[*Corresponding author] Tel: 86-25-85427544, E-mail: jiangyancpu@126.com (JIANG Yan); Tel: 86-25-83271382, Fax: 86-25-83271379, E-mail: cpuli@163.com (LI Hui-Jun)
These authors have no conflict of interest to declare.

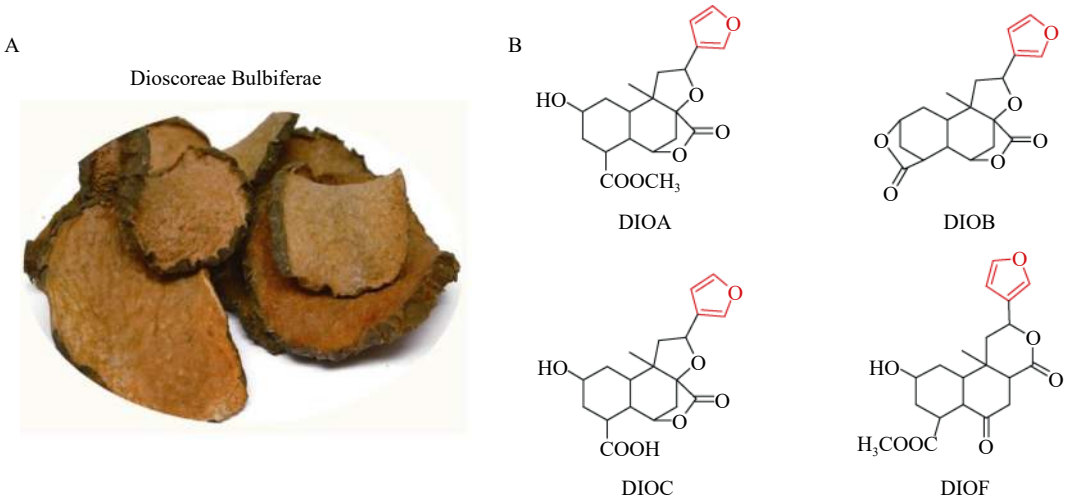

Fig. 1 Dioscoreae Bulbiferae (A) and chemical structures of DIOA, DIOB, DIOC, DIOF (B)

attributed to the metabolic oxidation of the furan ring [21-22] and CYP3A4 is the most effective enzyme for catalyzing the formation of the electrophilic intermediate [23]. Furthermore, recent findings suggested that DIOB-GSH conjugates were detected both *in vitro* [24] and *in vivo* [25]. However, the knowledge regarding the hepatotoxicity of other DLs is still limited.

In order to confirm the crucial factors that lead to differences in hepatotoxicity, four DLs (DIOA, DIOB, DIOC, DIOF) (Fig. 1B) were examined in the present study by evaluating the *in vitro* cytotoxicity of these compounds in L02 normal human liver cells, HepG2 hepatocarcinoma cells, HepG2 hepatocarcinoma cells with over expression of CYP3A4 and L02 cells with over expression of CYP3A4. Lactate dehydrogenase (LDH) release activity was also determined. Molecular docking was carried out to simulate the different interactions between these DLs and key metabolic enzymes and validate the regulatory role of metabolism and metabolic enzymes in differential hepatotoxicity. Furthermore, ultra liquid chromatography quadrupole time-of-flight mass spectrometry (UPLC-QTOF-MS) and ultra liquid chromatography triple-quadrupole tandem mass spectrometry (UPLC-QqQ-MS) were used to analyze the intermediates that were produced from the DLs and quantify GSH consumption during the metabolism, respectively. Based on the obtained results of this study, we found that reactive intermediates played an important role in DLs-induced toxicity and the regulation of metabolism may be the crucial determinant to explain the toxic mechanism and varied hepatotoxicity of DLs.

Materials and Methods

Reagents and materials

The DB sample was purchased from Yunnan Province, China. The sample was authenticated by Prof. LI Hui-Jun and deposited at the State Key Laboratory of Natural Medicines, China Pharmaceutical University. In our previous research, four DLs (DIOA, DIOB, DIOC and DIOF) were isolated from DB, and their chemical structures were confirmed by mass spectrometry, ^{1}H and ^{13}C NMR. The purity of each compound was determined to be greater than 98% by high performance liquid chromatography. Ketoconazole (KTZ), acetaminophen (AP) and dimethyl sulfoxide (DMSO) were purchased from Sigma-Aldrich (St. Louis, MO, USA). The Cell Counting Kit-8 (CCK-8), reduced glutathione (GSH) and glutathione reduced ethyl ester (Internal Standard, IS) were available from MCE (Shanghai, China). Antibodies against CYP3A4 were obtained from ABclonal (Abclonal, China) and *β*-actin was purchased from Servicebio Technology Company (Wuhan, China). HPLC-grade acetonitrile, methanol, and formic acid were obtained from Merck (Damstadt, Germany). Deionized water was prepared using a Milli-Q purification system (Millipore, Milford, MA, USA).

Cell culture

HepG2 cells were originally obtained from the American Type Culture Collection (ATCC), and the L02 normal human liver cells were purchased from the Institute of Biochemistry and Cell Biology Sciences (Shanghai, China). CYP3A4 overexpressed L02 cells and HepG2 cells were obtained from our previous study [7]. Dulbecco's modified Eagle's medium (DMEM) and fetal bovine serum (FBS) were obtained from Gibco (Grand Island, NY, USA). These cells were cultured in (DMEM) supplemented with 10% FBS, 100 $U \cdot mL^{-1}$ penicillin, and 100 $\mu g \cdot mL^{-1}$ streptomycin at 37 °C in a humidified atmosphere with 5% CO_2.

Preparation of Samples

The DLs standards and AP were each dissolved in DMSO to a concentration of 200 $mmol \cdot L^{-1}$ and AP was used as the positive control to evaluate the cytotoxicity. GSH was diluted with DMEM to a final concentration of 10 $mmol \cdot L^{-1}$ to capture the metabolic intermediates of the DLs. The concentrations of DMSO did not exceed 0.5% in all of the cell experiments.

Western Blot Analysis

HepG2 cells, L02 cells and CYP3A4 overexpressed L02

cells were seeded in 6-well plates at the density of 2 × 10^5 cells per well and cultured in 5% CO_2 at 37 °C for 24 h. All of the cells were lysed with ice-cold lysis buffer. Protein concentrations were measured using a protein assay kit (Bio-Rad, Hercules, CA, USA) according to the manufacturer's instructions. Extracted proteins were subjected to sodium dodecyl sulfate-polyacrylamide gel electrophoresis (SDS-PAGE) and transferred to polyvinylidene difluoride (PVDF) membranes (Millipore, Billerica, MA, USA). The immunoblot was probed with rabbit anti-CYP3A4 antibody diluted 1:1000, and mouse anti-*β*-actin antibody diluted 1 : 1000. Proteins were detected by chemiluminescence.

Cytotoxicity of L02, HepG2, CYP3A4 overexpressed L02 and HepG2 cells

Cell viability was determined by the CCK-8 assay. Cells were seeded in 96-well plates at the density of 1 × 10^4 cells per well and cultured in 5% CO_2 at 37 °C for 24 h. Then, the L02 cells, HepG2 cells, CYP3A4 overexpressed L02 and HepG2 cells were treated with four DLs standards (12 – 400 μmol·L^{-1}), and the other three groups in this experiment were set as follows: the solvent control group with 0.5% DMSO, the positive control group with 1 mmol·L^{-1} AP, the DLs + KTZ group with 12–400 μmol·L^{-1} DLs and 10 μmol·L^{-1} KTZ (KTZ was added 2 h before the CYP3A4 overexpressed L02 and HepG2 cells were treated with the DLs). After incubation for 48 h, the cells were treated with CCK-8 solvent of 10 μL per well for another 1 h, then the cells were detected with a microplate reader (BMG POLAR star Omega, Germany) to obtain the absorbance at 450 nm. The cell viability was calculated as follows: cell viability (%) = *OD* of DLs group or positive control group/*OD* of solvent control group × l00. The OD is presented as the means ± SD (n = 3) from three independent experiments.

LDH Assay

Lactate dehydrogenase leakage from cells was applied to estimate the toxic potential of harmful compound at the cellular level. CYP3A4 overexpressed L02 cells were seeded into 24-well plates at a density of 1 × 10^5 cells per well. After 24 h, CYP3A4 overexpressed L02 cells were exposed to DLs at the concentration of 100 μmol·L^{-1} for another 48 h. At the end of treatment, culture medium was collected and centrifuged at 3 000 r·min^{-1} for 5 min in order to obtain a cell free supernatant. The CYP3A4 overexpressed L02 cells in each well were also collected and washed twice with cold phosphate buffered saline (PBS) solution and Triton-X 100 was added at a final concentration of 1% to lyse the cells. Furthermore, a cell free supernatant was obtained after centrifuging at 13 000 r·min^{-1} for 10 min. Cell supernatants underwent an LDH assay using a commercially available kit from Nanjing Jiancheng Bioengineering Institute. The percentage of LDH leakage was calculated with the equation: LDH leakage (%) = [LDH activity in supernatant/LDH activity in (supernatant + cells)] × 100.

Molecular modeling of P450 3A4 and DLs docking studies

The 2D structures of the 4 ligands were drawn in ChemBioDraw 2013 and converted to 3D in Molecular Operating Environment (Molecular Operating Environment software, Chemical Computing Group Inc., Canada) through energy minimization. The CYP3A4 protein structure was downloaded from the Research Collaboratory for Structural Bioinformatics (RCSB) Protein Data Bank (PDB code: 5A1R) and prepared with the Structure Preparation workflow in MOE to fix structural issues such as missing residues/atoms or non-standard atom names. The protonation state of the protein and the orientation of the hydrogens were optimized by LigX, at the pH of 7 and temperature of 300 K. Prior to docking, the force field of AMBER10: EHT and the implicit solvation model of Reaction Field (R-field) were applied. The flexible docking workflow was carried out using MOE-dock following the "induced fit" protocol, in which the side chains of the receptor pocket were allowed to move according to ligand conformations, with a constraint on their positions. The weight used for tethering side chain atoms to their original positions was 10. For each ligand, all docked poses were ranked by London dG scoring first, and then, a force field refinement was carried out on the top 50 poses followed by a rescoring of GBVI/WSA dG, respectively. The top 10 remaining poses were further evaluated by visual inspection.

Trapping the GSH-conjugates in CYP3A4 overexpressed L02 cells

The UPLC-QTOF-MS method

UPLC-QTOF-MS analysis to screen the GSH-conjugates was carried out on a Waters Synapt G2 Q-TOF system (Waters, Manchester, USA) with an Acquity UPLC HSS C_{18} column (2.1 mm × 100 mm, 1.8 μm; Waters) and the column temperature was set at 35 °C. The mobile phase consisted of a mixture of 0.1% formic acid in water (phase A) and acetonitrile (phase B) at a flow rate of 0.2 mL·min^{-1}. The gradient elution program was optimized as follow: 95%–70% solvent A for 16 min, followed by 70%–15% solvent A for 4 min, and 15%–95% solvent A for 5 min. The solvent delay time was set to 5 min and the injection volume was set at 2 μL. The mass spectrometer was operated in positive ion mode with electrospray ionization (ESI) source and the mass spectrometer parameters were set as follow: capillary voltage, 3.0 kV; cone voltage, 20 V; source temperature, 120 °C; desolvation temperature, 400 °C; cone gas flow, 50 L·h^{-1}; and desolvation gas flow, 600 L·h^{-1}. The data were analyzed by MassLynx V4.1.

Sample preparation

The CYP3A4 overexpressed L02 cells were seeded in 6-well plates at the density of 2 × 10^5 cells per well and cultured in 5% CO_2 at 37 °C for 24 hours. Then, the cells were treated with four DLs and GSH, with the final concentration of the DLs in the cell system at 100 μmol·L^{-1} and the final concentration of GSH (dissolved in DMEM) at 10 mmol·L^{-1}. After 12 h of post-treatment, the GSH-conjugates were isolated by collecting the cell supernatant from the CYP3A4 overexpressed L02 cells. To remove precipitated protein, ice-cold acetonitrile was added to the collected supernatant.

The reaction mixture was vortex mixed and centrifuged at 13 000 r·min^{-1} for 10 min. The supernatants (800 μL) were air-dried with nitrogen and residues were reconstituted with 10% acetonitrile (100 μL). The resulting samples were injected into the UPLC-QTOF-MS for analysis.

GSH consumption assay in CYP3A4 overexpressed L02 cells

UPLC-QqQ-MS/MS analytical condition and method validation

Detections were carried out on an Agilent 1290 LC system coupled with an Agilent 6460 QqQ Mass Spectrometer (Agilent Technologies, Palo Alto, CA, USA). For separation, samples analysis was performed with an Acquity UPLC HSS C_{18} column (2.1 mm × 100 mm, 1.8 μm; Waters). The mobile phase adopted for this study was 0.1% formic acid in water (phase A) and acetonitrile (phase B) (10 : 90, *V*/*V*) at a flow rate of 0.4 mL·min^{-1}. The mass spectrometer was operated in positive ion mode with an electrospray ionization (ESI) source. Multiple-reaction monitoring (MRM) was chosen to quantify the GSH. The main mass spectrometer parameters were: drying gas temperature, 325 °C; drying gas flow, 10 L·min^{-1}; sheath gas temperature, 300 °C; sheath gas flow, 10 L·min^{-1}; nebulizer pressure, 35 psi; and capillary voltage, 3.5 kV. Data collection and processing were conducted with MassHunter Workstation 5.00 (Agilent Technologies, CA, United States).

The stock solution of GSH and IS were prepared in acetic acid-ammonium acetate buffer solution (pH = 4). Working standard solutions were prepared by diluting the stock solution into different concentrations ranging from 10 to 5000 ng·mL^{-1} and each also contained 1 μg·mL^{-1} of IS. Quality control (QC) samples at low, middle, and high concentrations were also prepared in the same way. All working solutions were stored at 4 °C before use. The method was fully validated according to the US Food and Drug Administration (FDA) guidelines in terms of selectivity, linearity, limit of quantification (LOQ), accuracy, precision, extraction recovery and matrix effect.

Sample preparation

Cellular GSH was determined using a UPLC-QqQ-MS method. The CYP3A4 overexpressed L02 cells that seeded in 6-well plates were treated with four DLs standard solutions at the concentration of 100 μmol·L^{-1} for another 48 h, and the control group was treated with 0.5% DMSO. At the end of the incubation, cell samples were washed with PBS twice and collected. The GSH of cells was extracted with acetic acid-ammonium acetate buffer solution (pH = 4) after ultrasonic treatment and then centrifuged at 13 000 r·min^{-1} for 10 min at 4 °C. Acetonitrile (450 μL) was added to the supernatant (150 μL) to precipitate the protein and the obtained supernatant was dried under nitrogen. The residues were reconstituted with 100 μL of ammonium acetate solution. After vortex-mixing for 1 min, the samples were centrifuged at 13 000 r·min^{-1} for 10 min at 4 °C. The resulting supernatant was injected into the UPLC-QqQ-MS system for analysis. The protein concentration was determined with protein quantification kit and the GSH levels are expressed as ng·mL^{-1} per mg protein.

Statistical analysis

All data are expressed as the mean ± SD. Figures were obtained with GraphPad Prism 5 (GraphPad Software, Inc., CA, USA). Statistical analyses were performed using SPSS 19 (IBM Corp., NY, USA). The statistical analysis was performed using one-way analysis of variance (ANOVA) with Dunnett's post hoc test to determine the significance of the differences between the individual groups. In the case of non-normally distributed data, Tamhane's T2 statistics was performed. A value of $P < 0.05$ was considered as statistically significant.

Results

CYP3A4 enzyme expression and cytotoxicity of DLs in L02, HepG2, CYP3A4 overexpressed L02 and HepG2 cells

In our previous study, we constructed L02 and HepG2 cells that overexpressed CYP3A4 enzyme. In order to verify the expression of the CYP3A4 enzyme in these cells, the western blot assay was used. Fig. 2 clearly shows that the CYP3A4 expression level in CYP3A4 overexpressed L02 and HepG2 cells was higher than that in wild-type L02 and

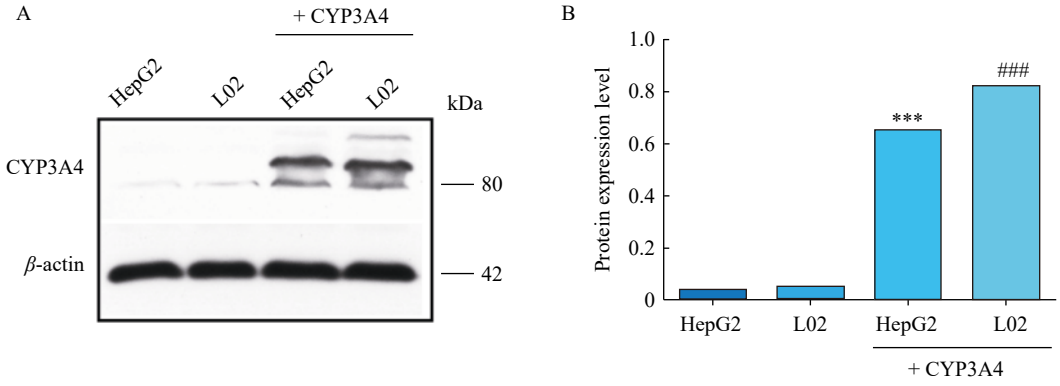

Fig. 2 Wild-type HepG2, L02 and stable CYP3A4 overexpressed L02, HepG2 cells underwent Western blot with CYP3A4 antibody(A). Statistical analysis. Expression of each protein was adjusted to actin as the loading control (B). All the experiments were repeated three times. $^{***}P < 0.01$ *vs* wild-type HepG2 cells; $^{\#\#\#}P < 0.01$ *vs* wild-type L02 cells

HepG2 cells.

The investigation results of the suitable administration time are shown in the supplementary materials (Fig. S1). The cytotoxicity results showed that after treated with DIOA or DIOF for 48 h, the cell viability of CYP3A4 overexpressed L02 cells was decreased more significantly than that treated with DIOA or DIOF for 24 h. To assess the cytotoxicity of DLs in wild-type L02 cells and CYP3A4 overexpressed L02 cells, the DLs were separately administered at concentrations from 12–400 μmol·L^{-1} for 48 h. The cell viability was compared with the wild-type L02 cells treated with DLs and CYP3A4 overexpressed L02 cells treated with DLs + KTZ. The results are shown in Fig. 3. The cell viability of CYP3A4 overexpressed L02 cells treated with DIOA was decreased in a concentration dependent manner compared with the control group and a highly significant statistical difference was observed among the wild-type L02 cells and CYP3A4 overexpressed L02 cells treated with DIOA at the concentration of 12 –400 μmol·L^{-1}. When the CYP3A4 overexpressed L02 cells were treated with DIOA + KTZ (10 μmol·L^{-1}), the cytotoxicity of DIOA (12 –400 μmol·L^{-1}) co-treated with KTZ was significantly decreased by 7.79%–39.19% in comparison with the DIOA sole group (Fig. 3A). While significant differences in cell viability among the wild-type and CYP3A4 overexpressed L02 cells exposed to DIOB was not seen until concentrations exceeded 25 μmol·L^{-1}. When the KTZ was added and co-treated with DIOB in the CYP3A4 overexpressed L02 cells, the cytotoxicity of DIOB was significant decreased at the concentration of 50, 100, 200 and 400 μmol·L^{-1} (Fig. 3B). The effect of DIOC on the cell viability of CYP3A4 overexpressed L02 cells was significantly decreased only at concentrations of 200 and 400 μmol·L^{-1} compared to the control group. Additionally, the cytotoxicity of these two types of cells exposed to DIOC showed significant differences at 200 and 400 μmol·L^{-1} and in the presence of KTZ, the cell viability of CYP3A4 overexpressed L02 cells was remarkably increased (Fig. 3C). After treatment with DIOF, the CCK-8 assay showed that DIOF elicited significant cytotoxic effects on the CYP3A4 overexpressed L02 cells compared with the wild-type cells and the cell viability was decreased in a concentration-dependent manner. At the same time, it was clear that when CYP3A4 overexpressed L02 cells were co-treated with DIOF and KTZ, the cell viability significantly increased at each dose from 12 – 400 μmol·L^{-1} (Fig. 3D).

Furthermore, the DLs were also separately administered at concentrations from 12–400 μmol·L^{-1} for 48 h in wild type HepG2 and CYP3A4 overexpressed HepG2 cells. The res-

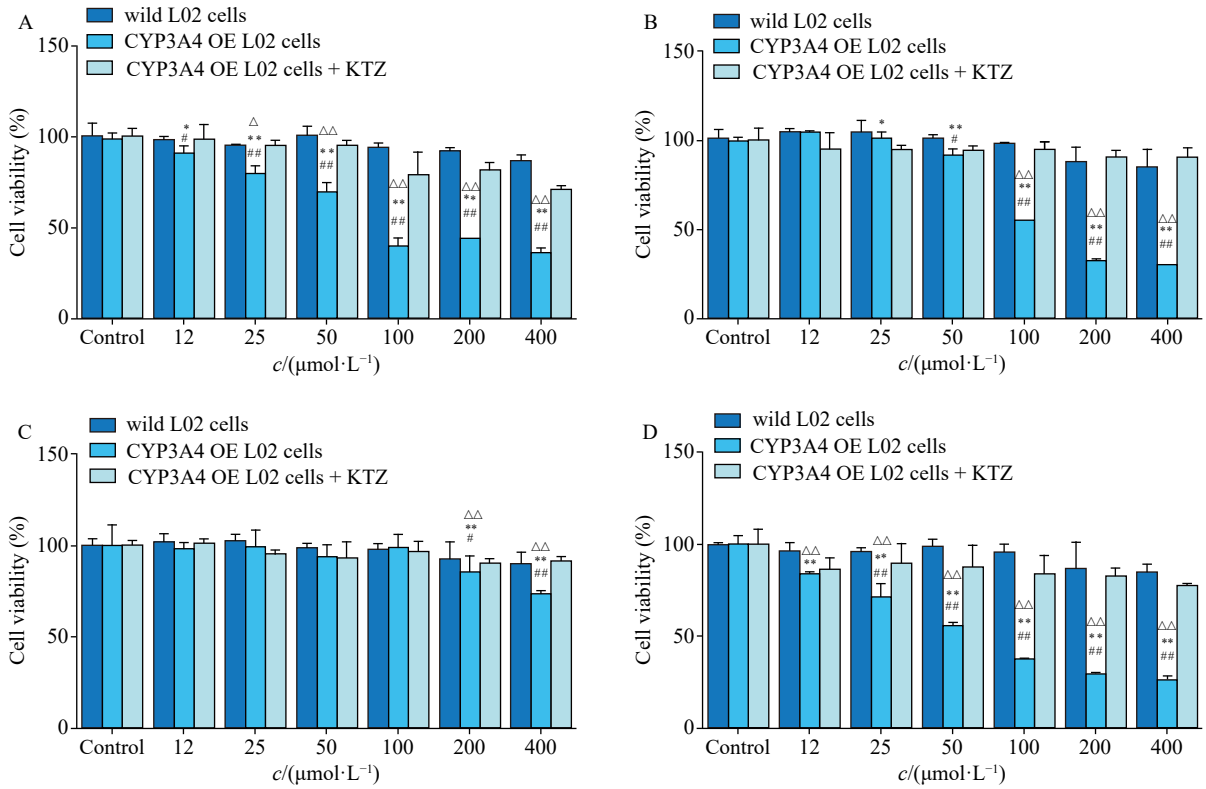

Fig. 3 Cytotoxicity of various concentrations of DLs on wild-type L02 cells, CYP3A4 overexpressed L02 cells and effect of various concentrations of DLs + KTZ on CYP3A4 overexpressed L02 cells. The CYP3A4 overexpressed L02 cells treated with DLs *vs* the control group, $^{\triangle}P < 0.05$, $^{\triangle\triangle}P < 0.01$; The CYP3A4 overexpressed L02 cells treated with DLs *vs* the wild-type L02 cells, $^{*}P < 0.05$, $^{**}P < 0.01$; The CYP3A4 overexpressed L02 cells treated with DLs *vs* the CYP3A4 overexpressed L02 cells treated with DLs + KTZ, $^{\#}P < 0.05$, $^{\#\#}P < 0.01$ Data are represented as mean ± SD of three independent experiments.

ults are shown in Fig. 4. The cell viability of CYP3A4 overexpressed HepG2 cells treated with DIOA at the concentration higher than 50 μmol·L^{-1} was significantly decreased compared with the wild type HepG2 cells. When the CYP3A4 overexpressed HepG2 cells were treated with DIOA and KTZ, the cytotoxicity of DIOA was decreased (Fig. 4A). While significant differences in cell viability among the wild-type and CYP3A4 overexpressed HepG2 cells exposed to DIOB was not seen until concentrations exceeded 100 μmol·L^{-1}. When the KTZ was added and co-treated with DIOB in the CYP3A4 overexpressed HepG2 cells, the cytotoxicity of DIOB was also significant decreased (Fig. 4B). However, DIOC showed no significant toxic effect both on wild type HepG2 and CYP3A4 overexpressed HepG2 cells (Fig. 4C). After treated with DIOF, the CCK-8 assay showed that DIOF elicited significant cytotoxic effects on the CYP3A4 overexpressed HepG2 cells compared with the wild-type cells. It was also obvious that KTZ could significantly increase the cell viability and decreased cytotoxicity of DIOF (Fig. 4D). These results suggested that the cytotoxicity of DLs was strengthened in CYP3A4 overexpressed cells and the toxic effects were weakened when the CYP3A4 overexpressed activity was inhibited by KTZ.

The IC_{50} values of the DLs in CYP3A4 overexpressed L02 cells were calculated (Supplementary Table S1). It is obvious that the order of IC_{50} is as follow: DIOC > DIOB > DIOA > DIOF. As an important basis for investigating the cytotoxicity of compounds in cell lines, we can preliminarily infer that the toxic effects of DLs on over expressed L02 cells.

LDH Release Assay

For further investigating the relationship between toxicity and reactive metabolites of these compound, we selected the concentration of 100 μmol·L^{-1} for subsequent experiments according to the IC_{50} values of the DLs in CYP3A4 overexpressed L02 cells. Here, the LDH release was another indicator of cell membrane damage and combined with cytotoxicity experiments were aimed to make the *in vitro* toxicity results more reliable. The results were shown in Fig. 5A. LDH release increased in different levels with 100 μmol·L^{-1} DLs treatment compared with solvent control group ($^{*}P < 0.05$, $^{**}P < 0.01$). As the positive control, the significant increase of LDH release induced by AP(1 mmol·L^{-1}) was observed. In the main time, the values of LDH release among the DLs showed significant differences and can be arranged in the following order: DIOF > DIOA > DIOB > DIOC. As a reference, the cell viabilities of the CYP3A4 overexpressed L02 cells treated by different DLs at 100 μmol·L^{-1} were shown in Fig. 5B. As expected, it also showed a significant difference and the toxic effects of the compounds obtained by

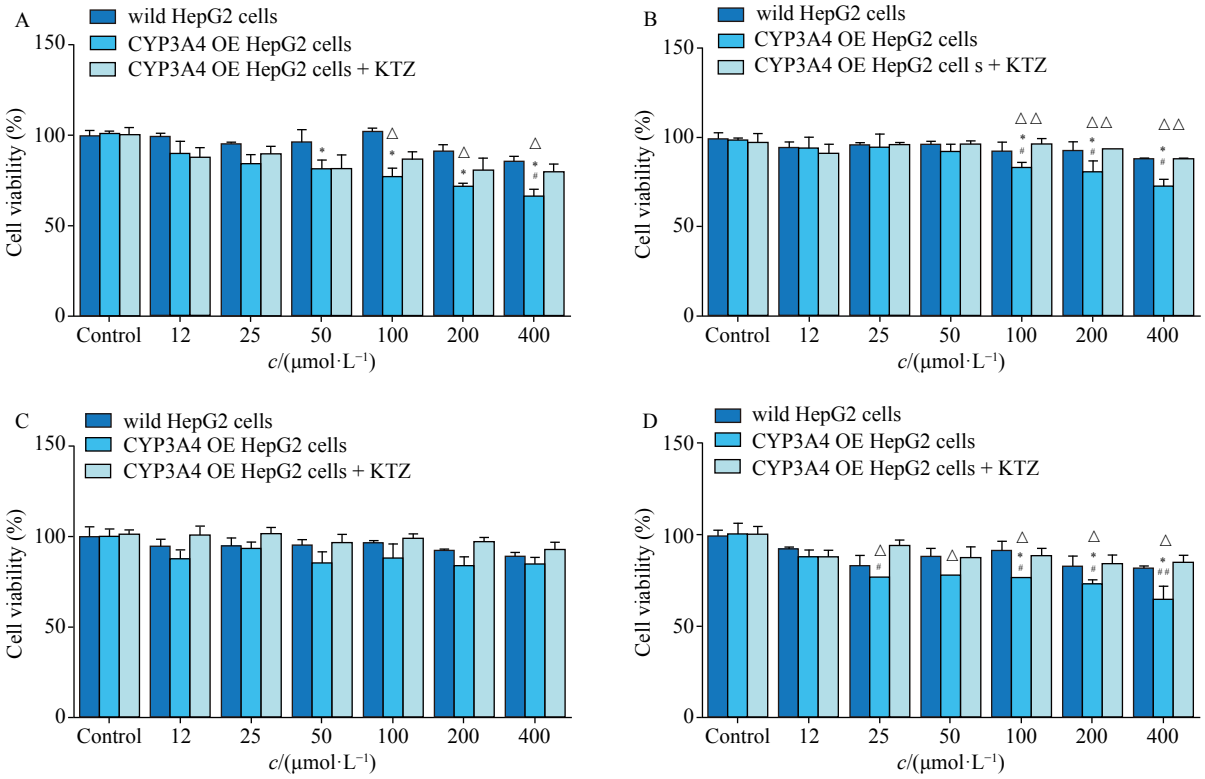

Fig. 4 Cytotoxicity of various concentrations of DLs on wild-type HepG2 cells, CYP3A4 overexpressed HepG2 cells and effect of various concentrations of DLs + KTZ on CYP3A4 overexpressed HepG2 cells. The CYP3A4 overexpressed HepG2 cells treated with DLs *vs* the control group, $^{\triangle}P < 0.05$; The CYP3A4 overexpressed HepG2 cells treated with DLs *vs* the wild-type HepG2 cells, $^{*}P < 0.05$; The CYP3A4 overexpressed HepG2 cells treated with DLs *vs* the CYP3A4 overexpressed HepG2 cells treated with DLs + KTZ, $^{\#}P < 0.05$, $^{\#\#}P < 0.01$ Data are represented as mean ± SD of three independent experiments.

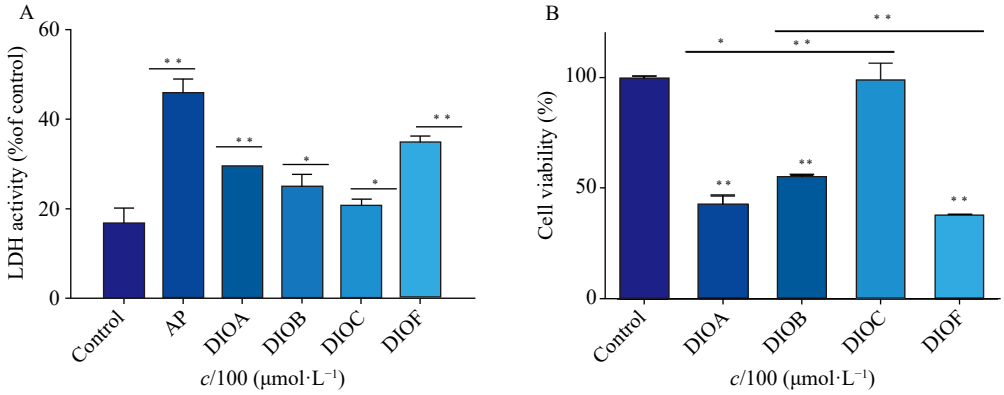

Fig. 5 Cytotoxicity was evaluated on CYP3A4 overexpressed L02 cells by LDH release assay, each DLs was at the concentration of 100 μmol·L^{-1} (A); Effect of DLs on the cell viability of CYP3A4 overexpressed L02 cells at the concentration of 100 μmol·L^{-1}. (B) (DLs and AP versus control; $^{*}P < 0.05$, $^{**}P < 0.01$). Data are represented as mean ± SD of three independent experiments.

the CCK8 assay showed the same trend with the results obtained from the LDH assay. Therefore, we could initially determine the strength of toxicity between these DLs at 100 μmol·L^{-1}.

Interactions of DLs bound to CYP3A4: different binding abilities

Through molecular docking of the four ligands with CYP3A4 (PDB code: 5A1R). The binding site of 5A1R was reported to be the peripheral site [26-27]. The estimated binding free energies indicated by GBVI/WSA dG scoring and the key residues of interactions are listed in Table 1. DIOF was predicted to be more potent (lower binding free energy scores) than the other compounds, and the trend is relatively consistent with our experiments.

To study the active binding mode and structure activity relationship (SAR), we compared the binding poses of the four compounds. The molecular surface for the binding pocket was also rendered and colored by polarity and hydrophobicity, as shown in Fig. 6. The secondary structure of the pocket is depicted as a ribbon representation. In general, DIOF and DIOA fit the pocket well in shape and form, with hydrophobic interactions at both the left and right sides of the pocket. Especially the methyl group to the right end of the pocket may form hydrophobic interactions with L482. Evidence for this was that DIOC is similar to DIOA in structure except for the lack of this methyl group, and DIOC cannot maintain the similar conformation, which was the probable reason for its inferior potency. Also, DIOB cannot fully occupy the two sides of the pocket, which lead to relatively weak affinity compared with DIOF and DIOA. Additionally, the carbonyl group of DIOF formed strong hydrogen bond with Asp214, which was conserved in the co-crystal structure of PDB 5A1R and probably renders DIOF more potent than others. The docking results of DLs bound to CYP3A4 showed a consistent relationship between the strength of affinity and the intensity of toxicity.

Identification of DLs-GSH conjugates

Several studies have confirmed that toxicity caused by compounds with a furan ring requires metabolism, and that the reactive metabolite is efficiently trapped with GSH [28-30]. We subsequently speculated that the furan ring of DLs is an important factor in DLs-induced liver injury, and specifically, that DLs were metabolized to the corresponding *cis*-enedione. The resulting electrophilic metabolite was responsible for the hepatotoxicity, and therefore, GSH was added to capture the active intermediates. As shown in Fig. 7, the adducts generated by binding to GSH are summarized according to the results. The mass spectral data for all the metabolites and the prototype of the DLs are listed in Table 2.

Several studies have confirmed that the mass fragmentation patterns of metabolites are similar to the parent compound, therefore the analysis of fragmentation pattern of par-

Table 1 Summary of docking results

Ligands	Total score (kcal·mol^{-1})	Interaction	
		H-bond	Key residues (4.5 Å)
DIOF	–6.63	Asp214	Asp214, Asp217, Arg212, Cys239, Ile238, Lys209, Leu482, Leu211, Pro242, Phe213, Phe219, Phe220, Val240
DIOA	–6.13	None	Asp214, Asp217, Arg212, Cys239, Ile238, Lys209, Leu482, Leu211, Phe213, Phe219, Phe220, Val240
DIOB	–5.89	None	Asp214, Asp217, Arg212, Cys239, Lys209, Leu482, Phe213, Phe219, Phe220, Val240
DIOC	–5.79	None	Asp214, Asp217, Arg212, Cys239, Lys209, Leu482, Leu211, Phe213, Phe219, Phe220, Phe241, Pro242, Val240

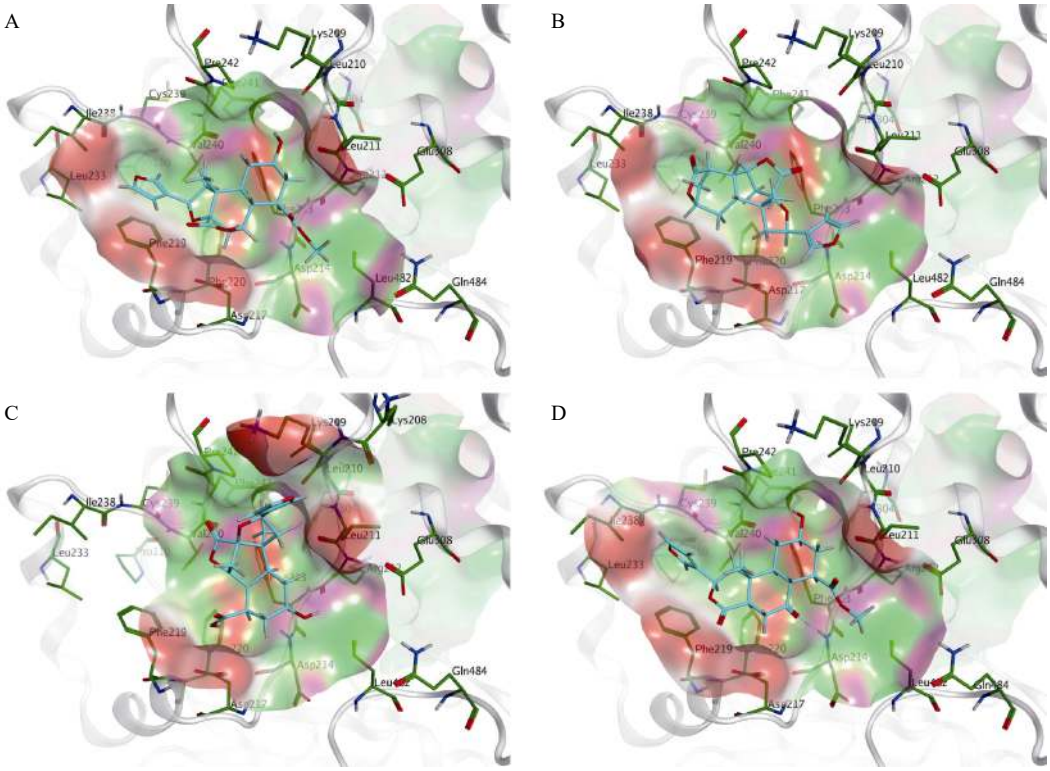

Fig. 6 The binding mode of the six compounds complexed with CYP3A4: (A) DIOA, (B)DIOB, (C) DIOC, (D) DIOF. The CYP3A4 backbone is shown with white ribbons, the ligand and the binding pocket residues of CYP3A4 are shown with stick representations, with the receptor colored in dark green and the ligand colored in cyan. The surface of the binding site is also depicted and colored in red (solvent exposed), magenta (polar), and light green (hydrophobic).

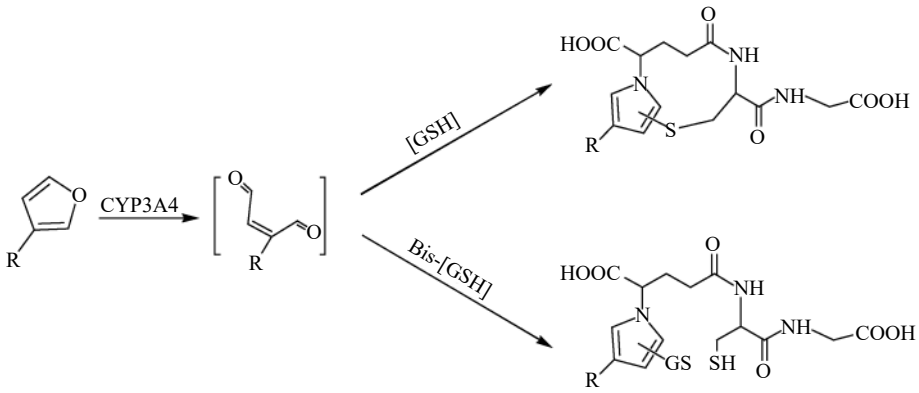

Fig. 7 Metabolic profile of DLs trapped by GSH

ent compound is very important for the metabolite characterizations [31]. The typical total ion chromatograph (TIC) and product ion spectrum of DIOA to DIOF are shown in Supplementary Fig. S2–S5. For example, DIOA provided a sodium adduct ion $[M + Na]^+$ at *m/z* 399, and the mass spectrum showed major fragment ions at *m/z* 331 ($-CH_2O_2$), 271 ($-C_2H_4O_2$), 253 ($-H_2O$) and 159 ($-C_6H_6O$). The metabolites named A1, A2, A3 and A4 were observed at *m/z* 664.7 $[M + H]^+$ with a chemical formula of $C_{30}H_{37}N_3O_{12}S$ by Q-TOF-MS, which indicated that one molecule of GSH might be conjugated to DIOA (Fig. 8A). The MS/MS spectra showed three major fragment ions (Fig. 8C), indicating that the product ions at *m/z* 647 and 589 were derived from the loss of the hydroxyl (–17 Da) and the glycine portion (–75 Da) from *m/z* 664, while another fragment ion at *m/z* 561 was derived from the loss of the carbonyl (–28 Da) from *m/z* 589. According to the synthesis of conjugates of teucrin A with *N*-acetyl lysine [32], the configuration of C12 in DIOA could change in the metabolites. Thus, A1 to A4 might be isomers with configurations changed in C12. In addition, another metabolite A5 was detected, and showed its molecular ion at *m/z* 971.3 $[M + H]^+$ (Fig. 8B); its formula was $C_{40}H_{54}O_{18}N_6S_2$. The formation of bis-GSH adducts of furan, indicated that two molecules of GSH might conjugate to DA. The *m/z* 896 and

Table 2 Mass spectral data for the metabolites and DLs

Compound	Formula	Adduct type	Exptl (*m*/*z*)	Calcd (*m*/*z*)	Error (ppm)	Fragment ions (*m*/*z*)
DIOA	$C_{19}H_{24}O_7$	$[M + Na]^+$	399.1394	399.1414	–5.0	331.1, 313.1, 295.1, 281.1, 253.1
A 1–A 4	$C_{30}H_{37}O_{12}N_3S$	$[M + H]^+$	664.2118–664.2163	664.2171	–4.2[a]	647.2, 589.2, 561.2
A5	$C_{40}H_{54}O_{18}N_6S_2$	$[M + H]^+$	971.2943	971.3009	–6.8	896.2, 664.2, 159.2
DIOB	$C_{19}H_{20}O_6$	$[M + NH4]^+$	362.1581	362.1604	–6.4	317.1, 299.1, 271.1, 253.1, 161.1
B 1–B 5	$C_{29}H_{33}N_3O_{11}S$	$[M + H]^+$	632.1879–632.1901	632.1914	–3.9[a]	615.2, 557.2, 529.2, 231.2
B 6	$C_{39}H_{50}O_{17}N_6S_2$	$[M + H]^+$	939.2722	939.2747	–2.7	864.2, 810.2, 632.2
DIOC	$C_{19}H_{22}O_7$	$[M + Na]^+$	385.1229	385.1263	–8.8	317.1, 299.1, 253.1, 159.1
C 1	$C_{29}H_{35}N_3O_{12}S$	$[M + H]^+$	650.1980	650.2041	–9.4	633.2, 575.2, 547.2, 159.2
DIOF	$C_{20}H_{24}O_7$	$[M + H]^+$	377.1585	377.1595	–2.7	345.1, 299.1, 281.1, 271.1, 253.1
F 1	$C_{30}H_{37}O_{12}N_3S$	$[M + H]^+$	644.2081	664.2130	–7.4	647.2, 589.2, 561.2
F 2	$C_{40}H_{54}O_{18}N_6S_2$	$[M + H]^+$	971.2981	971.3009	–2.9	926.2, 896.2, 664.2

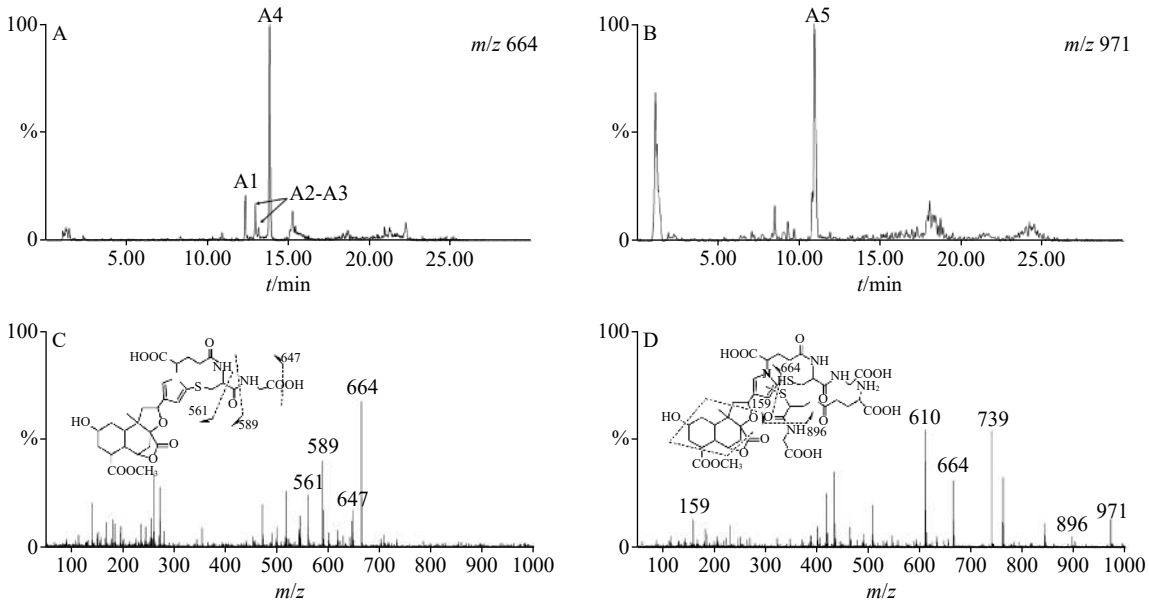

Fig. 8 Extracted ion (*m*/*z* 664) (A), (*m*/*z* 971) (B) chromatograms obtained from UPLC-QTOF-MS analysis of CYP3A4 overexpressed L02 cells incubations containing DIOA, GSH. (C) MS/MS spectrum of A1-A4, generated in incubations system. (D) MS/MS spectrum of A5 generated in incubations system

664 were the two major fragment ions derived from the loss of the glycine portion (–75 Da) and a part of GSH (–307 Da) from *m*/*z* 971.3 (Fig. 8D). Unfortunately, the yield of metabolites is extremely low and it is not possible to collect a sufficient amount for nuclear magnetic resonance characterization.

In all, five mono-GSH adducts (B1 –B5) and one bis-GSH–derived conjugate (B6) of DIOB were detected in the incubation system in the presence of GSH (Supplementary Fig. S6). In the incubation system of DIOC and DIOF, one mono-GSH adduct (C1 and F1) as well as a bis-GSH adduct (F2) were respectively detected (Supplementary Fig. S7–S8). All the GSH adducts were detected and characterized based on accurate mass measurement, the fragmentation pattern of the parent compounds and relevant drug biotransformation knowledge.

Method Validation for UPLC-QqQ-MS/MS

Representative MRM chromatograms of the blank hepatocytes sample, blank hepatocytes sample spiked with the standard solutions and the hepatocytes sample treated with DLs are shown in Supplementary Fig. S9. No endogenous interfering peaks were observed in the hepatocytes sample at the measured mass transitions and retention times of the analytes and IS for the highly selective MRM mode.

The results for linearity, LOQ, accuracy, precision, recoveries and matrix effect are exhibited satisfactory results (Supplementary Table S2 –S4). Calibration exhibited satisfactory linearity ranging from 0.01 to 5 μg·mL^{-1} with correla-

tion coefficient (r) at 0.997. The LOQ of GSH was 10 ng·mL^{-1}. The intra- and inter-day precision and accuracy were less than 15%, indicating that the accuracy and precision of the method were acceptable for quantitative analysis. The mean recoveries of GSH ranged from 91.50% to 98.68% at three concentration levels. This demonstrated that the sample preparation method could ensure the acquisition of accurate and consistent data. The matrix effect was between 104.38% and 109.44%, which suggested that there was no significant ion suppression in this method.

Effects of DLs on the Hepatocytes Concentrations of GSH

The concentrations of GSH in the hepatocytes samples were measured by UPLC-QqQ-MS. The results of the assay were then adjusted to protein and the final intracellular GSH content is expressed as the amount of GSH per mg of protein. The remaining GSH in the system after treatment with DLs at the same condition is shown in Fig. 9. We observed a significant decrease in the GSH content in the cells compared with the control group and there were significant differences in the GSH content in cells treated with the four DLs. The values of GSH consumption could be arranged in the following order: DIOF > DIOA > DIOB > DIOC. Compared with the results of CCK-8 and LDH analysis, the most significant revelation from the measurements was that GSH consumption was positively correlated with the effects of toxicity.

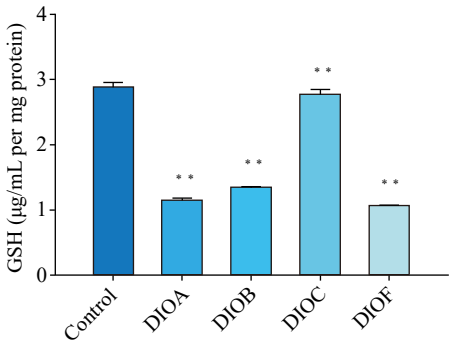

Fig. 9 Cellular GSH after treated by DLs (DLs, *vs* control on CYP3A4 overexpressed L02 cells, $^{**}P < 0.01$). Data are represented as mean ± SD of three independent experiments.

Discussion

The present study attempted to confirm the potential factors that impact the toxicity of DLs to provide reasonable explanations for the differential hepatotoxicity. The cytotoxicity of DLs was evaluated *in vitro*. The results of cell experiments showed that the toxic effects were not obvious on wild-type L02 and HepG2 cells compared to the CYP3A4 overexpressed L02 and HepG2 cells. When the CYP3A4 enzyme in the CYP3A4 overexpressed cells was inhibited, the toxic effects were significantly decreased because the KTZ is a selective CYP3A4 inhibitor [33]. Our observation was in accordance with previous studies that reported the CYP3A4 enzyme in the cells enhanced the toxicity of DIOB [34]. It indicated that the mechanism of toxicity may be closely related to metabolism and metabolic enzymes play an important role in the regulation of toxicity. In addition, other studies have shown that DB exhibited significant antitumor activity in mice inoculated with 180 sarcoma cells, but no activity in a tumor cell line *in vitro* due to low CYP expression in cell lines [35]. It was also reported that cytotoxicity is usually difficult to predict *in vitro* due to the differences in CYP expression caused by drug-metabolizing enzymes [36] and even in liver cancer HepG2 cells [37]. The data were consistent with our results for wild-type cells. Cytotoxicity results showed that DLs showed more significant toxic effects on CYP3A4 overexpressed L02 cells compared to CYP3A4 overexpressed HepG2 cells. Therefore, we preferred to use the CYP3A4 overexpressed L02 cells rather than the normal cell lines and CYP3A4 overexpressed HepG2 cells to investigate the differential cytotoxicity and potential cytotoxic mechanism of DLs-induced *in vitro*. The IC_{50} values of the CCK-8 assay for CYP3A4 overexpressed L02 cells preliminarily demonstrated the difference of toxic effects.

Furthermore, cell necrosis or membrane damage produced by toxicants can lead to leakage of LDH from cells and result in increased LDH activity in cell supernatant [38]. Therefore, the LDH activity measured for CYP3A4 overexpressed L02 cells was used to further evaluate the cytotoxicity of these DLs in order to obtain more reliable results. For the LDH activity assay, we only selected the concentration at 100 μmol·L^{-1} for each DLs, due to the fact that a suitable dose of the DLs should be considered to use in the subsequent cell experiments according to the IC_{50} values. In addition, the main purpose of the LDH assay was to further confirm the intensity of toxic effects at this concentration. As expected, the results of the LDH assay showed the same trend of cytotoxicity as that of the CCK-8 assay at 100 μmol·L^{-1}. These results provided accurate cytotoxicity data for investigating the relationship between metabolic intermediates and toxicity in subsequent experiments.

Molecular docking studies were used to understand the interaction between a ligand and a target protein or enzyme at the atomic level [39]. This method was used in our research to investigate whether different structures of small molecules affected the ability to bind to an enzyme, thereby influencing the oxidation metabolism of a furan ring. As expected, the molecule with the preferred conformation incorporated DIOF and DIOA, the combination of which gained a higher score than that for DIOB and DIOC. It was demonstrated that the main goal of the scoring functions was to estimate the binding affinity of a compound with the protein [39-40]. According to the results of molecular docking, combined with the results verified by cell experiments, we preliminarily confirmed that structures with dominant conformation may have a stronger interaction with metabolic enzymes, which in turn may promote the metabolic oxidation of furan ring to produce higher toxicity. Unfortunately, due to the fact that the number of compounds and the toxicity data are limited, we

can only give a brief explanation about the structure-activity relationships that DLs with a six-membered ring in the structure are more likely to maintain a stable conformation. Whether there is a direct link between the structures and hepatotoxicity needs further verification.

Adduct formation was thought to be an important trigger to the toxic effects with the reactive intermediate 's chemical [8]. Consequently, to verify the toxic mechanism of DLs, UPLC-QTOF-MS was used to analyze the intermediates that were produced by the DLs due to its high resolution and sensitivity of, which made it possible to detect various types of main trace components in complex systems [41]. Because furan epoxide intermediates were difficult to isolate for chemical characterization, the structures of the reactive metabolites of DLs were confirmed by the structural elucidations of metabolites in the trapping experiments of GSH and similar methods that were previously reported [8, 21, 23]. B1–B5 (*m*/*z* 632.2) and B6 (*m*/*z* 939.2) were inferred to be DIOB, combined with one and two molecules of GSH, respectively. In other words, the two kinds of metabolites were produced by the reaction of cis-enedial oxidative metabolite with the nitrogen (glutamate residue) and the sulfur (cysteine residue) of the same molecule of GSH and our observations were in accordance with previous studies [21, 23]. For other DLs, the cytotoxic mechanism may be similar to that of DIOB because of similar groups in their molecular structures. Therefore, their structures were speculated according to the mass spectrometry data. Fortunately, on the basis of the high-resolution molecular ion and MS/MS spectra, we observed two types of GSH-derived adducts. One type was mono-GSH reaction products composed of one molecular of GSH and the parent compound such as A1-A4, C1and F1-F2. Another type was the DLs conjugated to bis-GSH, and these were found in the system of DIOA and DIOF. According to the synthesis of conjugates of teucrin A with N-acetyl lysine [32], the configuration of C12 in DLs could change in the metabolites and it may be a reasonable reason to explain the multiple mono-GSH conjugates of DIOA and DIOB. As the multiple metabolites produced by DIOA and DIOB are the isomers, the mass spectrum showed nearly the same major fragment ions. Due to this fact that we selected a representative mass spectrum to demonstrate the structural characteristics of the reactive metabolites. Although it was difficultly to determine the adducts that each peak corresponded to, the structural elucidations from the mass data have shown us that the mechanism of toxicity induced by these DLs is mainly related to the oxidation of furan rings. These results further confirmed that metabolic regulation is a crucial factor in generating hepatotoxicity.

In addition, GSH plays an important role in modulating the toxicity. In many cases, the reactive intermediates derived from furan ring oxidation may conjugate to GSH to form an adduct in the absence of glutathione *S*-transferases [8]. In the current study, the detection of DLs−GSH adducts revealed that GSH adduct formation might be a critical event involved in the development of DLs-induced liver injury. Due to the reactive intermediates were unstable that we cannot quantify the metabolic intermediates directly. Based on this fact that we determined the amount of intracellular GSH after administration of the same dose of DLs and compared the results to the cytotoxicity of DLs to indirectly reflect the relationship between reactive metabolic intermediates and hepatotoxicity. UPLC-QqQ-MS was used to quantify the cellular GSH, and when we analyzed the GSH consumption in association with the cytotoxicity of DLs, we found that there was a consistent relationship between them. The system with more GSH consumption showed a stronger toxic effect and vice versa. As mentioned before, cytochrome P450 catalyzed the furan ring oxidation to form a *cis*-enedione, and this was the main metabolic pathway that caused toxic effects. The results indicated that under the same conditions, the ability of furan ring oxidation metabolism in DLs to produce different amount of reactive intermediates, and therefore, the effects of hepatotoxicity may be correspondingly different.

Currently, except DIOB there are no relevant reports on the *in vivo* hepatotoxicity of the DLs that mentioned in this article. Study showed that administration of DIOB produced acute liver injury by biochemical estimation of serum markers and histopathological examination [22]. In particular, biotransformation of the furan group played an important role in DIOB hepatotoxicity [23]. P450 3A was the primary enzyme that catalyzes the metabolic activation of DIOB and toxicological studies consistently showed that pretreatment with ketoconazole protected the animals from hepatotoxicity [42]. These reports are consistent with the results of the *in vitro* hepatotoxicity in this article. Experiments on hepatotoxicity induced by DLs *in vivo* should be carried out in subsequent studies and combined with the *in vitro* studies can help us better understand the liver injury induced by DLs.

In summary, the crucial role of metabolic regulation in DLs-induced differential hepatotoxicity was successfully confirmed and the toxic mechanism of DLs was uncovered. Compounds with more active intermediates generated through the pathway of furan ring oxidation are more toxic than others and metabolic enzymes play a modulatory role in this process. This study may be greatly helpful in elucidating the toxic effects of DLs in DB and provides reference for the early diagnosis and tracing of possible furanoids-induced liver injury.

Abbreviations

Acetaminophen (AP); Cell counting kit-8 (CCK-8); cytochrome P450 (CYP); Chinese herbal medicines (CHMs); Diterpenoid lactones (DLs); *Dioscorea bulbifera* L. (DB); diosbulbin A (DIOA); diosbulbin B (DIOB); diosbulbin C (DIOC); diosbulbin F (DIOF); Dimethyl sulfoxide (DMSO); Dulbecco's modified Eagle 's medium (DMEM); Electrospray ionization (ESI); Fetal bovine serum (FBS); glutathione (GSH); Ketoconazole (KTZ); Limit of quantification (LOQ); Lactate dehydrogenase (LDH); Multiple-reaction monitoring (MRM); Polyvinylidene difluoride (PVDF); Phosphate buf-

fered saline (PBS); Quality control (QC); Sodium dodecyl sulfate-polyacrylamide gel electrophoresis (SDS-PAGE); typical total ion chromatograph (TIC); ultra liquid chromatography quadrupole time-of-flight mass spectrometry (UPLC-QTOF-MS); ultra liquid chromatography triple-quadrupole tandem mass spectrometry (UPLC-QqQ-MS).

Supplementary materials

Supporting Information of this paper can be requested by sending e-mails to the corresponding author

References

[1] Moser GJ, Foley J, Burnett M, *et al*. Furan-induced dose− response relationships for liver cytotoxicity, cell prolif-eration, and tumorigenicity (furan-induced liver tumorigenicity) [J]. *Exp Toxicol Pathol*, 2009, **61**(2): 101–111.

[2] Dong H, Gill S, Curran IH, *et al*. Toxicogenomic assessment of liver responses following subchronic exposure to furan in Fischer F344 rats [J]. *Arch Toxicol*, 2016, **90**(6): 1351–1367.

[3] Kalgutkar AS, Gardner I, Obach RS, *et al*. A comprehensive listing of bioactivation pathways of organic functional groups [J]. *Curr Drug Metab*, 2005, **6**(3): 161–225.

[4] Khojasteh-Bakht SC, Chen W, Koenigs LL, *et al*. Metabolism of (*R*)-(+)-pulegone and (*R*)-(+)-menthofuran by human liver cytochrome P-450s: evidence for formation of a furan epoxide [J]. *Drug Metab Dispos*, 1999, **27**(5): 574–580.

[5] Sztajnkrycer MD. Mitigation of pennyroyal oil hepatotoxicity in the mouse [J]. *Acad Emerg Med*, 2003, **10**(10): 1024–1028.

[6] Lu X, Ji C, Tong W, *et al*. Integrated analysis of microRNA and mRNA expression profiles highlights the complex and dynamic behavior of toosendanin-induced liver injury in mice [J]. *SCI REP-UK*, 2016, **6**: 34225.

[7] Li ZQ, Jiang LL, Zhao DS, *et al*. The modulatory role of CYP3A4 in dictamnine-induced hepatotoxicity [J]. *Front Pharmacol*, 2018, **9**: 1033.

[8] Peterson LA. Reactive metabolites in the biotransformation of molecules containing a furan ring [J]. *Chem Res Toxicol*, 2013, **26**(1): 6–25.

[9] Chen L, Liao H, Chen P, *et al*. Limonoids from the seeds of swietenia macrophylla and their anti-inflammatory activities [J]. *Molecules*, 2015, **20**(10): 18551–18564.

[10] Lee D, Jeon E, Ahn J, *et al*. Limonin enhances osteoblastogenesis and prevents ovariectomy-induced bone loss [J]. *J Funct Foods*, 2016, **23**: 105–114.

[11] Gao H, Kuroyanagi M, Wu L, *et al*. Antitumor-promoting constituents from *Dioscorea bulbifera* L. in JB6 mouse epidermal cells [J]. *Biol Pharm Bull*, 2002, **25**(9): 1241–1243.

[12] Guan X, Zhu L, Xiao Z, *et al*. Bioactivity, toxicity and detoxification assessment of *Dioscorea bulbifera* L.: a comprehensive review [J]. *Phytochem Rev*, 2017, **16**(3): 573–601.

[13] Wang J, Liang Q, Ji L, *et al*. Gender-related difference in liver injury induced by *Dioscorea bulbifera* L. rhizome in mice [J]. *Hum Exp Toxicol*, 2010, **30**(9): 1333–1341.

[14] Teschke R, Larrey D, Melchart D, *et al*. Traditional chinese medicine (TCM) and herbal hepatotoxicity: rucam and the role of novel diagnostic biomarkers such as microRNAs [J]. *Medicines*, 2016, **3**(3): 18.

[15] Rakotobe L, Mambu L, Deville A, *et al*. Clerodane and 19-norclerodane diterpenoids from the tubers of dioscorea antaly [J]. *Phytochemistry*, 2010, **71**(8-9): 1007–1013.

[16] Liu H, Chou G, Guo Y, *et al*. Norclerodane diterpenoids from rhizomes of *Dioscorea bulbifera* [J]. *Phytochemistry*, 2010, **71**(10): 1174–1180.

[17] Peterson LA. Glutathione trapping to measure microsomal oxidation of furan to cis-2-butene-1, 4-dial [J]. *Drug Metab Dispos*, 2005, **33**(10): 1453–1458.

[18] Lu D, Peterson LA. Identification of furan metabolites derived from cysteine-*cis*-2-butene-1, 4-dial-lysine cross-links [J]. *Chem Res Toxicol*, 2010, **23**(1): 142–151.

[19] Dalvie DK, Kalgutkar AS, Khojasteh-Bakht SC, *et al*. Biotransformation reactions of five-membered aromatic heterocyclic rings [J]. *Chem Res Toxicol*, 2002, **15**(3): 269–299.

[20] Teponno RB, Tapondjou AL, Gatsing D, *et al*. Bafoudiosbulbins A, and B, two anti-salmonellal clerodane diterpenoids from *Dioscorea bulbifera* L. var *sativa* [J]. *Phytochemistry*, 2006, **67**(17): 1957–1963.

[21] Feng S, He X. Mechanism-based inhibition of CYP450: an indicator of drug-induced hepatotoxicity [J]. *Curr Drug Metab*, 2013, **14**(9): 921–945.

[22] Li W, Lin D, Gao H, *et al*. Metabolic activation of furan moiety makes diosbulbin B hepatotoxic [J]. *Arch Toxicol*, 2016, **90**(4): 863–872.

[23] Yang B, Liu W, Chen K, *et al*. Metabolism of diosbulbin B *in vitro* and *in vivo* in rats: formation of reactive metabolites and human enzymes involved [J]. *Drug Metab Dispos*, 2014, **42**(10): 1737–1750.

[24] Lin D, Li C, Peng Y, *et al*. Cytochrome P450-mediated metabolic activation of diosbulbin B [J]. *Drug Metab Dispos*, 2014, **42**(10): 1727–1736.

[25] Li C, Lin D, Gao H, *et al*. *N*-acetyl lysine/glutathione-derived pyrroles as potential *ex vivo* biomarkers of bioactivated furan-containing compounds [J]. *Chem Res Toxicol*, 2015, **28**(3): 384–393.

[26] Sevrioukova IF, Poulos TL. Anion-dependent stimulation of CYP3A4 monooxygenase [J]. *Biochemistry*, 2015, **54**(26): 4083–4096.

[27] Williams PA. Crystal structures of human cytochrome P450 3A4 bound to metyrapone and progesterone [J]. *Science*, 2004, **305**(5684): 683–686.

[28] Lu D, Sullivan MM, Phillips MB, *et al*. Degraded protein adducts of cis-2-butene-1, 4-dial are urinary and hepatocyte metabolites of furan [J]. *Chem Res Toxicol*, 2009, **22**(6): 997–1007.

[29] Shi FG, Pan H, Cui BD, *et al*. Dictamnine-induced hepatotoxicity in mice: the role of metabolic activation of furan [J]. *Toxicol Appl Pharm*, 2018, **364**: 68–76.

[30] Khojasteh-Bakht SC, Oishi S, Nelson SD. Metabolism and toxicity of menthofuran in rat liver slices and in rats [J]. *Chem Res Toxicol*, 2010, **23**(11): 1824–1832.

[31] Wang L, Ye H, Sun D, *et al*. Metabolic pathway extension approach for metabolomic biomarker identification [J]. *Anal Chem*, 2017, **89**(2): 1229–1237.

[32] Druckova A, Marnett LJ. Characterization of the amino acid adducts of the enedial derivative of teucrin A [J]. *Chem Res Toxicol*, 2006, **19**(10): 1330–1340.

[33] Zahno A, Brecht K, Bodmer M, *et al*. Effects of drug interactions on biotransformation and antiplatelet effect of clopidogrel *in vitro* [J]. *Brit J Pharmacol*, 2010, **161**(2): 393–404.

[34] Jiang J, Yang B, Ji L, *et al*. Metabolic-induced cytotoxicity of diosbulbin B in CYP3A4-expressing cells [J]. *Toxicol in Vitro*, 2017, **38**: 59–66.

[35] Komori T. Glycosides from *Dioscorea bulbifera* [J]. *Toxicon*, 1997, **35**(10): 1531–1536.

[36] Grillo MP. Detecting reactive drug metabolites for reducing the potential for drug toxicity [J]. *Expert Opin Drug Metab Toxicol*, 2015, **11**(8): 1281–1302.

[37] Westerink WMA, Schoonen WGEJ. Cytochrome P450 en-

zyme levels in HepG2 cells and cryopreserved primary human hepatocytes and their induction in HepG2 cells [J]. *Toxicol in Vitro*, 2007, **21**(8): 1581–1591.

[38] Roh T, De U, Lim SK, *et al*. Detoxifying effect of pyridoxine on acetaminophen-induced hepatotoxicity *via* suppressing oxidative stress injury [J]. *Food Chem Toxicol*, 2018, **114**: 11–22.

[39] Malathi K, Ramaiah S. Bioinformatics approaches for new drug discovery: a review [J]. *Biotechnol Genet Eng Rev*, 2018, **34**(2): 243–260.

[40] Muegge I, Martin YC. A general and fast scoring function for protein−ligand interactions: a simplified potential approach [J]. *J Med Chem*, 1999, **42**(5): 791–804.

[41] Castro-Perez J, Plumb R, Granger JH, *et al*. Increasing throughput and information content for in *vitro* drug metabolism experiments using ultra-performance liquid chromatography coupled to a quadrupole time-of-flight mass spectrometer [J]. *Rapid Commun. Mass Spectrom*, 2005, **19**(6): 843–848.

[42] Wang K, Lin DJ, Guo XC, *et al*. Chemical identity of interaction of protein with reactive metabolite of diosbulbin B *in vitro* and *in vivo* [J]. *Toxins*, 2017, **9**(8): 249.

Cite this article as: WU Zi-Tian, LI Zhuo-Qing, SHI Wei, WANG Ling-Li, JIANG Yan, LI Ping, LI Hui-Jun. The crucial role of metabolic regulation in differential hepatotoxicity induced by furanoids in *Dioscorea bulbifera* [J]. *Chin J Nat Med*, 2020, **18**(1): 57-69.